UCRL-ID-144571-PT-2

A Fast Running Test Bed Model to Evaluate Atmospheric Plume Source Properties II: Source Location Inversion Sensitivity Tests

A.S. Grossman, C.F. Molenkamp, K.E. Grant

June 1, 2001

U.S. Department of Energy

Lawrence Livermore National Laboratory

DISCLAIMER

This work was performed under the auspices of the U. S. Department of Energy by the University of California, Lawrence Livermore National Laboratory under Contract No. W-7405-Eng-48.

A FAST RUNNING TEST BED MODEL TO EVALUATE ATMOSPHERIC PLUME SOURCE PROPERTIES. II: SOURCE LOCATION INVERSION SENSITIVITY TESTS

Charles F. Molenkamp
Allen S. Grossman
Keith E. Grant

This work was performed under the auspices of the U.S. Department of Energy by the University of California Lawrence Livermore National Laboratory under Contract No. W-7405-Eng-48.

ABSTRACT

A technique has been developed to obtain selected source parameters for a release of toxic material into the atmosphere by inversion of a set of sensor observations. The technique utilizes the Marquardt inversion method coupled to a Gaussian puff atmospheric dispersion model. The major objective of this report is to perform a set of sensitivity calculations to explore the robustness of the source location inversion procedure to variations in source location relative to sensor location, spacing of sensors, sensor integration period, and sensor observation times. The results of the tests for variation of source location show that the inversion accuracy is sensitive to source placement relative to a rectangular sensor array with most accurate inversions occurring when the source is aligned with a downwind row of sensors and least accurate when the source is placed between downwind sensor rows. When the density of the sensor array was increased by a factor of 4, i.e. spacing cut in half, the case with the poorest source location inversion accuracy in the first test significantly improved. The results of tests for variation of sensor integration time show that the most accurate source location inversion occurs for the smallest integration time and the least accurate for the largest integration time. The results of tests for variation of the number of observations show that the most accurate source location inversion occurs for the case with the most observation times and the accuracy degrades as the number of observation times decreases. As a general rule throughout all of the sensitivity tests performed here, the most accurate source inversions occur when the number of data points (in both time and space) is maximized.

I. INTRODUCTION

A recent report (Grossman et al., 2001, "GMG") described a technique in which selected source properties for a toxic material released into the atmosphere are obtained by inversion of a set of measured concentrations. The technique utilizes the Marquardt inversion method coupled to a Gaussian puff atmospheric dispersion model (INtegrated PUFF, Petersen and Lavdas, 1986) driven by a COAMPS regional prognostic model (Hodur, 1997) wind field. The inversion results are used in conjunction with a probability model for 1000 sensor realizations to evaluate the reliability of the technique. A test scenario, based on a puff release of material within a 40 km x 40 km domain in the Salt Lake City, Utah area, was used to evaluate the inversion model. Source parameters selected for the test scenario were:

a. Source horizontal location, $x = 2$ km, $y = 20$km.
b. Source release start time, $t = 3600$s.
c. Source strength, $Q = 100$ g/s.
d. Puff duration, $D = 6$s (single puff).

Auxiliary parameters selected for INPUFF were:

a. Source release height = 1m.
b. Air Temperature = 296 K.
c. Stability Class = C (P-G Stability Class, particular relation for σ vs. downwind distance).
d. Mixing height = 1000 m.

Sensor placement (a rectangular array with sensors at the x/y intersections):

a. $x = 3, 11, 19, 27$ km (downwind),
b. $y = 12, 20, 28$ km (crosswind),
c. Sensor integration time = 5 minutes.

An initial guess for source location was determined via a 'backtrack' method as outlined in GMG. Assuming a particular release time, the backtrack technique estimates source location by calculating a backwards trajectory for each sensor with a non-zero concentration and then calculates the average or concentration weighted average (centroid) location.

To start each study a set of "truth" sensor readings are generated by running the INPUFF Gaussian puff dispersion model using the actual source parameters. The non-zero "truth" concentrations are then perturbed with random errors to provide a set of simulated observations (the inversion technique uses these observations; it does not know about "truth"). A realization is defined as a set of non zero sensor readings (both spatially and temporally) where each individual sensor reading includes a random perturbation of the "truth" value. Assume the

perturbed sensor readings follow a lognormal probability distribution about the "truth" concentration with a standard deviation, α. Each perturbed sensor reading will then have a probability based on a log normal distribution. The probability of the realization is the product of the individual sensor probabilities divided by the product of the probability of the realization where each sensor reads the "truth" values.

An inversion was performed for 1000 realizations, and these results were used to determine the source parameter probability distribution. In order to calculate the probability of the source location at any particular point, the x-y plane was divided into squares 0.1km on a side, centered on the true source location. The number of sensor realizations for which the source location occurs in a particular x–y square was tabulated and this number, divided by the total number of sensor realizations (normalization factor), was interpreted as the probability of the source being located in that square. The estimated release time and source strength was obtained by calculating the mean value for each quantity in the x–y square having the highest source location probability.

The results of the initial test calculations showed that the inversion procedure produced good results with reasonably well defined maximum probabilities for the four source properties (x, y, t, and Q) in a 1000 sensor realization scenario. The technique finds the source location, release time, and strength within ~±50 m, ~±10 s, and ~±10 g/s for the most probable values and within ~ ±300m, ~±25 s, and ~±45 g/s at the 90% confidence level.

The major objective of this report is to perform a set of sensitivity calculations to explore the robustness of the source location inversion procedure to variations in the following input parameters: source location, number of sensors, sensor integration time, and sensor reading times.

II. SENSITIVITY CALCULATION SCENARIOS

To explore the sensitivity of the inversion procedure to source location, the horizontal source location was varied in the y coordinate (approximately the crosswind direction);

$$x = 2 \text{ km}, y = 12 - 28 \text{ km } (\Delta y = 1 \text{ km}),$$

keeping all other problem parameters the same as those used by GMG (see above). Then the case where the source is located at $x = 2$ km and $y = 15$ km will be used with a sensor set which has a more dense spacing to explore the effect of sensor spacing on inversion accuracy. To explore the

effect of sensor integration time on the inversion procedure, sensor integration times of 5, 10, 20, 30, and 60 minutes were used for the case of a source located at x = 2 km and y = 15 km. To explore the sensitivity of the inversion model on the number of observations available, the following calculations were performed for a source located at x = 2 km and y = 15 km and a sensor integration time of 20 minutes;

a. use observation periods 1 (0–20 min.), 2 (20–40 min.), and 3 (40–60 min.),
b. use observation periods 1 and 2,
c. use observation periods 1 and 3,
d. use observation periods 2 and 3,
e. use observation period 2, and
f. use observation period 3.

Observation period 1 alone had too few non-zero values to perform an inversion. As was the case in GMG, each of the above sensitivity tests involved 1000 sensor realizations.

Two methodologies were considered in GMG for the calculation of sensor perturbations. The method used for the GMG calculations (Sample 1) consisted of a set of concentrations generated using a normal random number generator. With this method, each set of individual sensor readings, as well as the distribution of realizations, obeys a normal distribution. An alternative method (Sample 2) utilizes a linear random number generator to determine a perturbation to the actual sensor reading; then a probability, based on the log normal distribution, is determined for the individual perturbed sensor reading (Iman and Shortencarier, 1984). The first method automatically takes the sensor reading probabilities into account while the second method provides more concentrations in the wings of the probability distribution. The Sample 2 sensor perturbation methodology was chosen for use in this paper. With this method, the realization probabilities for each source location within a particular x–y square are summed to obtain the cumulative probability for the source location in the square. This probability is normalized by dividing by the probability of the "truth value" sensor realization. Since the major concern is the relative probabilities square to square, the normalization factors are of minor consequence. The estimated release time and source strength were obtained by calculating the probability weighted mean values for release time and source strength in the x–y square having the highest source location probability.

III. RESULTS AND DISCUSSION

The results for the first experiment in which the source location was moved in the crosswind direction from 12 km to 28 km, keeping x fixed at 2 km, and using the 8 km sensor spacing used in GMG, are summarized in Tables 1 and 2, and Figures 1, 2, and 3. Table 1 shows:

a. Number of realizations where the difference in the distance (m) between the source location obtained via the average backtrack method and via the centroid backtrack method is < 1m, < 10m, < 100m,
b. Number of times the estimated source location, out of 1000 realizations, is located < 25m, < 100m, < 200m, from the true source location for the centroid backtrack method,
c. Number of times the estimated source location, out of 1000 realizations, is located < 25m, < 100m, < 200m, from the true source location for the average backtrack method,
d. Number of times the estimated source is located more than 600m from the true source location for each backtrack method.

Inspection of Table 1 shows that inversion accuracy varies with both the y location of the source and the method used for calculation of the initial x–y guess. The first column of Table 1 is an estimate of the consistency between the two initial x–y guesses obtained by the centroid and average backtrack methods. In nine of the seventeen cases at least 700 of the 1000 sensor realization inversions yield estimated source x–y values which differ by less than 100m from each other. For three cases the number of sensor realizations yielding a distance difference less than 100m between estimated source x–y values for the two backtrack methods is less than ~50m. The second and third sections of Table 1 show the accuracy of the inverted source locations for the 1000 realizations, for each of the two backtrack methods, as the y value of the true source changes. Using the d < 100m column as the example, it can be seen that inversion accuracy varies as the true y value of the source varies. Inversion accuracy tends to be high when the source is aligned with a line of sensors (y = 12 km, 20 km, and 28 km) and also at y values of 17 and 25 km (the wind has a slight northerly component). Inversion accuracy tends to be lower when the y value of the source is ~13 – 16 km and ~21 – 24 km, i.e. when the true source is located between sensor lines. There is a definite repetition of the inversion accuracy pattern as the source is moved between sensor lines. Table 2 shows the number of sensors with non zero readings for the total one hour sampling period and the number of sensors with non zero reading for each of the twelve, five minute sampling periods. There is a definite correlation between the number of sensors involved in the inversion and inversion accuracy. The highest accuracy inversion (y = 17 km) is associated with the most sensors (14) having non zero values and the

lower values of inversion accuracy correspond to cases where the number of sensors involved in the inversion decreased to eight or nine sensors. Figure 1 shows the number of times out of 1000 realizations that the distance difference between estimated and true source locations is less than 100m plotted against the y value of the true source; also plotted is the number of sensors involved in each realization. The solid line (□) is the plot for source locations obtained via the average backtrack method, the dotted (◊) line is the plot for source locations obtained via the centroid backtrack method, and the dashed line (O) is proportional (n x 40) to the number of sensors involved in the realization. The vertical lines at 12 km, 20 km, and 28 km indicate the location of the sensor lines. The variation of inversion accuracy with y value of the source is clearly shown for both backtrack methods. While the centroid backtrack method produces slightly higher inversion accuracy when the source is aligned with one of the sensor lines, the average backtrack method produces higher inversion accuracy over the complete range of y values. In particular, the centroid backtrack method produces erroneous source locations for cases where the y value of the source is ~ 18—19 km and ~ 26—27 km. Overall, the average backtrack method provides initial x–y guesses which yield more accurate estimated source locations. Figure 1 also shows that inversion accuracy is directly related to the number of sensors involved in the inversion. Figure 2 shows the cumulative inversion probabilities in 100 meter per side squares in the x–y plane for the 1000 realizations. Figure 2a shows the plot for the case where the source is located at x = 2 km, y = 15 km and the initial x and y guess for the inversion model was obtained using the average backtrack method. This was a case which had very poor inversion accuracy. Figure 2a shows that the inversion appeared to converge at x = 1.2 km and y = 14.8 km. Figures 2b and 2c show plots for the case where the source is located at x = 2 km, y = 17 km and the initial x and y guesses for the inversion model were obtained using the average (2b) and the centroid (2c) backtrack methods. These cases had the highest inversion accuracy and the figures show that nearly all the sensor realizations produced inverted source locations close to the actual values. Figure 2d shows the plot for the case where the source is located at x = 2 km, y = 19 km and the initial x and y guess was obtained using the centroid backtrack method. As was the case in Figure 2a, this represents a case of poor inversion accuracy. The inversion appears to converge at x = 2.3 km and y = 23.6 km. Figures 2e and 2f show the plots for the case where the source is located at x = 2 km, y = 20 km and the initial x and y guesses for the inversion model were obtained using the average (2e) and the centroid (2f) backtrack methods. These cases show reasonably good inversion accuracy. We believe that poor accuracy occurs when the initial guess, as determined by the backtrack method, is far from the true source. Then the small variations in source location used in starting the Marquardt inversion do not provide a clear signal of what direction to move towards the true source. In essence, the X^2 function is quite flat and the Marquardt iteration gets caught in a local X^2 minimum. Figure 3 shows the log of the probability product for each of the 1000 sensor realizations as a function of distance

between inverted source location and true source location for the cases shown in Figure 2. Figure 3a shows the plot for the case where the source is located at $x = 2$ km, $y = 15$ km and the initial x and y guess for the inversion model was obtained using the average backtrack method. For this case a significant number of the 1000 realizations, including those with high probability products, cluster at an inverted distance ~1 km from the actual source. Apparently the initial, backtracked guess for the source location is in this region, and the Marquardt technique converges in a local X^2 minimum. Figures 3b and 3c show plots for the cases where the source is located at $x = 2$ km, $y = 17$ km and the initial x and y guesses for the inversion model were obtained using the average (3b) and the centroid (3c) backtrack methods. As discussed above, sensor realization probabilities are clustered within an inverted distance of 100—200m from the actual source. Figure 3c shows a few low probability points ~4 km from the true source. Figure 3d shows the plot for the case where the source is located at $x = 2$ km, $y = 19$ km and the initial x and y guess for the inversion model was obtained using the centroid backtrack method. This is another case where the inverted source values clustered about a point 4—5 km away from the actual point with high sensor realization probability. Figures 3e and 3f show the plots for the case where the source is located at $x = 2$ km, $y = 20$ km and the initial x and y guesses for the inversion model were obtained using the average (3e) and the centroid (3f) backtrack methods. This is the case considered by GMG. The results show a primary probability peak within 100m of the actual source as well as a secondary, lower probability peak ~400m from the actual source location. The secondary probability peak generated in the average backtrack method results of Figures 2e and 3e was not generated in the GMG results for the same case. We attribute this to the different sampling models used to generate the sensor realizations. The maximum probability peaks do occur at the same points for both sampling methods.

To explore the effect of sensor spacing on inversion we took the case where the source is located at $y = 15$ km and $x = 2$ km. As discussed above, this was a case where inversion accuracy for the GMG sensor set was poor. The sensor spacing was decreased from 8 km in the x and y directions to 4 km. A total of 48 sensors were used ($y = 10$—30 km, $\Delta y = 4$ km; $x = 1$—29 km, $\Delta x = 4$ km, '215B') compared to the 12 sensor array ('215A') for the above calculations. These two cases are compared in Table 3 (same format as Table 1). The first column of Table 3 shows that 998 of the 1000 inversion pairs yield inverted source x–y location differences of less than 100m for the initial x–y guesses obtained by the centroid and average backtrack methods. This compares to 179 of the 1000 inversions for the 8 km sensor set. Columns 2, 3, and 4 of Table 3 show very significant improvement in the inversion accuracy for the denser sensor array. Figures 4a (average backtrack method) and 4b (centroid backtrack method) show the cumulative inversion probabilities in 100 meter per side squares in the x–y plane for the 1000 realizations. Figure 4 shows that the inversion appeared to converge at $x = 2$ km and $y = 15$ km with a single, sharp probability peak, indicating very good accuracy.

Table 3. Results Of Inversion Calculations For 1000 Sensor Realizations Using Sensor Spacings of 8 km (A) and 4 km (B)

Run	Distance Difference			Accuracy (Centroid)			Accuracy (Average)			Outside ±600m	
	<1	<10	<100	<200	<100	<25	<200	<100	< 25	c	a
215A	69	124	179	455	206	27	110	24	0	239	806
215B	531	953	998	999	938	178	1000	939	174	1	0

Table 4. Results Of Inversion Calculations For 1000 Sensor Realizations As a Function Of Sensor Integration Time

Run	Distance Difference			Accuracy (Centroid)			Accuracy (Average)			Outside ±600m	
	<1	<10	<100	<200	<100	<25	<200	<100	<25	c	a
215/5	531	953	998	999	938	178	1000	939	174	1	0
215/10	548	916	998	998	862	114	998	857	118	1	0
215/20	545	888	980	949	633	69	966	644	64	0	0
215/30	306	779	965	686	254	24	676	255	22	0	0
215/60	344	791	998	646	212	12	638	213	13	0	1

Results for sensitivity tests of the source location inversion model to sensor integration time are shown in Table 4 (same format as Table 1) and Figures 4 and 5. These results assume the actual source location was x = 2 km and y = 15 km and use the 48 sensor array described above. Source inversions were performed for 1000 sensor realizations using sensor integration times of 5, 10, 20, 30 and 60 minutes. Table 4 shows that inversion accuracy degrades monotonically as integration time is increased. This is most probably due to the fact that the number of

observations used in the inversion calculation is also decreased. It is interesting to note that even at an integration time of 60 minutes the inversion accuracy is better with the 48 sensor array than the inversion accuracy with the 12 sensor array and a 5 minute integration time (see Table 3). Figures 5a (average backtrack method) and 5b (centroid backtrack method) show the cumulative inversion probabilities in 100 meter per side squares in the x–y plane for the 60 minute sensor integration case. Comparison of these figures with Figures 4a and 4b (5 minute sensor integration case) shows the 60 minute case probability distributions to be more spread out in the *x–y* plane, but there are no secondary probability peaks in either case.

Table 5. Results Of Inversion Calculations For 1000 Sensor Realizations Using Different Observation Times

Run	Distance Difference			Accuracy (Centroid)			Accuracy (Average)			Outside ±600m	
	<1	<10	<100	<200	<100	<25	<200	<100	<25	c	a
215/123	545	888	980	949	633	69	966	644	64	0	0
215/23	530	857	1000	948	537	55	947	531	52	0	0
215/13	283	509	799	824	402	23	965	552	34	0	0
215/12	334	497	523	870	455	38	486	224	20	1	465
215/2	602	917	993	847	324	32	845	327	32	0	0
215/3	379	642	995	658	234	16	659	228	18	0	1

The results for tests of sensitivity of source location inversion model to sensor observation time are shown in Table 5 (same format as Table 1) and Figures 6 and 7. The actual source location was $x = 2$ km and $y = 15$ km, and the 48 sensor array described above was used. The sampling period was 20 minutes and 1000 inversions were performed using sampler concentrations from time periods 1 (0—20 min), 2 (20—40 min), and 3 (40—60 min) as follows:

1,2,3 - Run 215/23,
2,3 - Run 215/23,
1,3 - Run 215/13,
1,2 - Run 215/12,
2 - Run 215/2,
3 - Run 215/3.

The most accurate of the above tests occurs when all three-observation periods are used in the source inversion calculation. The inversion which uses observation periods 2 and 3 is next in accuracy. There is a definite separation in accuracy between these two cases and the next three cases, 215/13, 215/12, and 215/2. The latter three cases all have about the same accuracy. For cases 215/13 and 215/12 there are significant differences in source location accuracy between the centroid and average backtrack methods. The 215/12 case using the average backtrack method yields a particularly poor inversion. The 215/3 case (observation period 3) is the least accurate in this sensitivity test. The general accuracy trend in Table 5 can be correlated with the number of data points available for the inversion in each case;

a. Case 215/123 - 17 data points,
b. Case 215/23 - 15 data points,
c. Case 215/13 - 12 data points,
d. Case 215/13 - 7 data points,
e. Case 215/2 - 10 data points,
f. Case 215/3 - 5 data points.

Figures 6a (average backtrack method) and 6b (centroid backtrack method) show the cumulative inversion probabilities in 100 meter per side squares in the x–y plane for the 1000 sensor realizations for the 215/123 case. Figures 7a (average backtrack method) and 7b (centroid backtrack method) show the cumulative inversion probabilities in 100 meter per side squares for case 215/3. The probability distributions for case 215/123 are sharper and of greater magnitude than those for case 215/3.

In summary, a series of sensitivity tests for the inversion model, developed by GMG, were run to explore the dependence of estimated source location on the y coordinate of the true source, the spatial density of the sensor array, sensor integration time, and number of observation times. Results of tests for variation of the y coordinate show that inversion accuracy is sensitive to source placement within the sensor array; the most accurate inversions occur when the source is aligned with a downwind row of sensors and least accurate inversions occur when the source is

placed between downwind sensor rows (see Figure 1). When the density of the sensor array was increased by a factor of 4, the low-resolution array case with the poorest estimated source location had a significant improvement in accuracy (see Table 3). Results of tests for variation of sensor integration time show that the most accurate source location estimate occurs for the smallest integration time and the least accurate for the largest integration time (see Table 4.). Tests on sensitivity of the inversion model to number of observations show that the most accurate source locations occur when all observation times are included and accuracy degrades as the number of observation times decreases (see Table 5). As a general rule throughout all of the sensitivity tests performed here, the most accurate source inversions occur when the number of data points (in both time and space) is maximized.

VI. REFERENCES

Edwards, L. L., R. P. Freis, L. G. Peters, and P. H. Gudiksen, 1992: The use of nonlinear regression analysis for integrating pollutant measurements with atmospheric dispersion modeling for source term estimation. *Nucl. Technol.*, **101**, 168.

Grossman, A. S., C. F. Molenkamp, and K. E. Grant, 2001: A fast running test bed model to evaluate atmospheric plume source properties. I: Initial test scenario. LLNL Report UCRL----, in press ('GMG').

Hodur, R, M., 1997: The Naval Research Laboratory's coupled ocean/atmosphere mesoscale prediction system (COAMPS). *Mon. Wea. Rev.*, **119**, 1414–1430.

Iman, R. L., and M. J. Shortencarier, 1984: A FORTRAN 77 program and user's guide for the generation of Latin Hypercube and random samples for use with computer models. SNL Report NUREG/CR-3624, SAND83-2365.

Petersen, W. B., and L. Lavadas, 1986: INPUFF 2.0—A multiple source Gaussian puff dispersion algorithm. EPA Report EPA-600/8-86/024.

Table 1. Accuracy and Distance Difference Frequency as a Function of Actual Source Location. There are 1000 Realizations for Each Source Location.

Table 2. Number of Non-Zero Readings for a Sampling Array With Twelve Sensors In Each 5 Minute Sampling Period.

FIGURE CAPTIONS

Figure 1. Number of source locations for 1000 sensor realizations having distance differences with respect to the true source location of less than 100m plotted against the y location of the true source. The solid line (□) is the plot of the source locations obtained via the average backtrack method, the dotted(◊) line is the plot for the source locations obtained via the centroid backtrack method, and the dashed line (O) is proportional (n x 40) to the number of sensors involved in the realization. The vertical lines at y = 12 km, 20 km, and 28 km indicate the y coordinate of sensor lines.

Figure 2a. Estimated source location probability histogram for 100m x 100m elements. The actual source is at x = 2 km, y = 15 km, initial guess uses average backtrack method, 12 sensor array (8 km spacing).

Figure 2b. Estimated source location probability histogram for 100m x 100m elements. The actual source is at x = 2 km, y = 17 km, initial guess uses average backtrack method, 12 sensor array (8 km spacing).

Figure 2c. Estimated source location probability histogram for 100m x 100m elements. The actual source is at x = 2 km, y = 17 km, initial guess uses centroid backtrack method, 12 sensor array (8 km spacing).

Figure 2d. Estimated source location probability histogram for 100m x 100m elements. The actual source is at x = 2 km, y = 19 km, initial guess uses centroid backtrack method, 12 sensor array (8 km spacing).

Figure 2e. Estimated source location probability histogram for 100m x 100m elements. The actual source is at x = 2 km, y = 20 km, initial guess uses average backtrack method, 12 sensor array (8 km spacing).

Figure 2d. Estimated source location probability histogram for 100m x 100m elements. The actual source is at x = 2 km, y = 20 km, initial guess uses centroid backtrack method, 12 sensor array (8 km spacing).

Figure 3a. Log of the probability product as a function of the distance between the inverted source location and the true source location for each of the 1000 realizations. Source is located at x = 2 km, y = 15 km and initial guess uses average backtrack method.

Figure 3b. Log of the probability product as a function of the distance between the inverted source location and the true source location for each of the 1000 realizations. Source is located at x = 2 km, y = 17 km and initial guess uses average backtrack method.

Figure 3c. Log of the probability product as a function of the distance between the inverted source location and the true source location for each of the 1000 realizations. Source is located at x = 2 km, y = 17 km and initial guess uses centroid backtrack method.

Figure 3d. Log of the probability product as a function of the distance between the inverted source location and the true source location for each of the 1000 realizations. Source is located at x = 2 km, y = 19 km and initial guess uses centroid backtrack method.

Figure 3e. Log of the probability product as a function of the distance between the inverted source location and the true source location for each of the 1000 realizations. Source is located at $x = 2$ km, $y = 20$ km and initial guess uses average backtrack method.

Figure 3f. Log of the probability product as a function of the distance between the inverted source location and the true source location for each of the 1000 realizations. Source is located at $x = 2$ km, $y = 20$ km and initial guess uses centroid backtrack method.

Figure 4a. Estimated source location probability histogram for 100m x 100m elements. The actual source is at $x = 2$ km, $y = 15$ km, initial guess uses average backtrack method, 48 sensor array (4 km spacing), with 5 minute averaging.

Figure 4b. Estimated source location probability histogram for 100m x 100m elements. The actual source is at $x = 2$ km, $y = 15$ km, initial guess uses centroid backtrack method, 48 sensor array (4 km spacing), with 5 minute averaging.

Figure 5a. Estimated source location probability histogram for 100m x 100m elements. The actual source is at $x = 2$ km, $y = 15$ km, initial guess uses average backtrack method, 48 sensor array (4 km spacing), with 60 minute averaging.

Figure 5b. Estimated source location probability histogram for 100m x 100m elements. The actual source is at $x = 2$ km, $y = 15$ km, initial guess uses centroid backtrack method, 48 sensor array (4 km spacing), with 60 minute averaging.

Figure 6a. Estimated source location probability histogram for 100m x 100m elements. The actual source is at $x = 2$ km, $y = 15$ km, initial guess uses average backtrack method, 48 sensor array (4 km spacing), with 20 minute averaging.

Figure 6b. Estimated source location probability histogram for 100m x 100m elements. The actual source is at $x = 2$ km, $y = 15$ km, initial guess uses centroid backtrack method, 48 sensor array (4 km spacing), with 20 minute averaging.

Figure 7a. Estimated source location probability histogram for 100m x 100m elements. The actual source is at $x = 2$ km, $y = 15$ km, initial guess uses average backtrack method, 48 sensor array (4 km spacing), with 20 minute averaging, uses only sensor data from 40—60 minutes after release.

Figure 7b. Estimated source location probability histogram for 100m x 100m elements. The actual source is at $x = 2$ km, $y = 15$ km, initial guess uses centroid backtrack method, 48 sensor array (4 km spacing), with 20 minute averaging, uses only sensor data from 40—60 minutes after release.

Table 1

Run	Distance Difference			Accuracy (Centroid)			Accuracy (Average)			Outside ± 600 m	
	< 1	< 10	< 100	< 200	< 100	< 25	< 200	< 100	< 25	c	a
212	401	665	760	600	408	38	514	358	30	0	186
213	260	421	641	631	392	64	734	467	79	240	133
214	88	245	518	286	125	19	271	135	18	232	217
215	69	124	179	455	206	27	110	24	0	239	806
216	294	380	389	713	311	10	288	77	3	57	592
217	264	625	916	897	568	75	960	629	77	49	0
218	85	164	263	258	127	13	924	489	43	731	0
219	7	12	19	20	10	0	730	453	53	980	0
220	659	777	798	712	575	84	598	493	75	0	29
221	265	557	757	426	242	21	428	252	24	247	325
222	452	770	884	303	108	6	337	108	7	185	157
223	414	885	999	690	288	26	687	282	25	2	1
224	750	964	1000	769	282	25	770	278	22	0	0
225	406	764	978	944	608	58	953	604	56	1	0
226	20	31	31	3	12	25	870	447	45	969	0
227	24	48	52	0	22	47	886	409	28	948	0
228	493	671	819	694	521	72	602	441	80	0	26

Table 1

Table 2

Time-> SRC Loc	0-5	5-10	10-15	15-20	20-25	25-30	30-35	35-40	40-45	45-50	50-55	55-60	Total
2, 10	0	0	0	0	1	1	1	1	2	2	2	1	11
2, 11	0	0	0	0	1	1	1	1	2	2	2	2	12
2, 12	1	1	0	0	1	1	1	1	1	2	2	2	13
2 13	1	1	0	0	1	1	1	1	1	2	2	2	13
2, 14	0	0	0	0	1	1	1	1	1	2	2	2	11
2, 15	0	0	0	0	0	1	1	1	1	2	2	2	10
2, 16	0	0	0	0	0	0	01	1	1	1	2	2	8
2 17	0	0	0	0	0	0	01	2	2	2	3	4	14
2, 18	0	0	0	0	0	0	1	2	2	2	2	4	13
2, 19	0	0	0	0	0	1	1	1	1	1	2	3	10
2, 20	1	1	1	0	0	1	1	1	1	1	2	2	12
2, 21	0	1	0	0	0	1	1	1	1	1	2	2	10
2, 22	0	0	0	0	0	1	1	1	1	1	2	2	9
2, 23	0	0	0	0	0	1	1	1	1	1	2	2	9
2, 24	0	0	0	0	0	0	1	1	1	1	2	2	8
2, 25	0	0	0	0	0	0	0	2	2	2	3	4	13
2, 26	0	0	0	0	0	0	1	1	2	2	2	4	12
2, 27	0	0	0	0	0	0	1	1	1	1	2	3	10
2, 28	1	1	1	0	0	1	1	1	1	1	2	2	12
2, 29	0	1	0	0	0	1	1	1	1	1	2	2	10
2, 30	0	0	0	0	0	1	1	1	1	1	2	2	9

Figure 1.

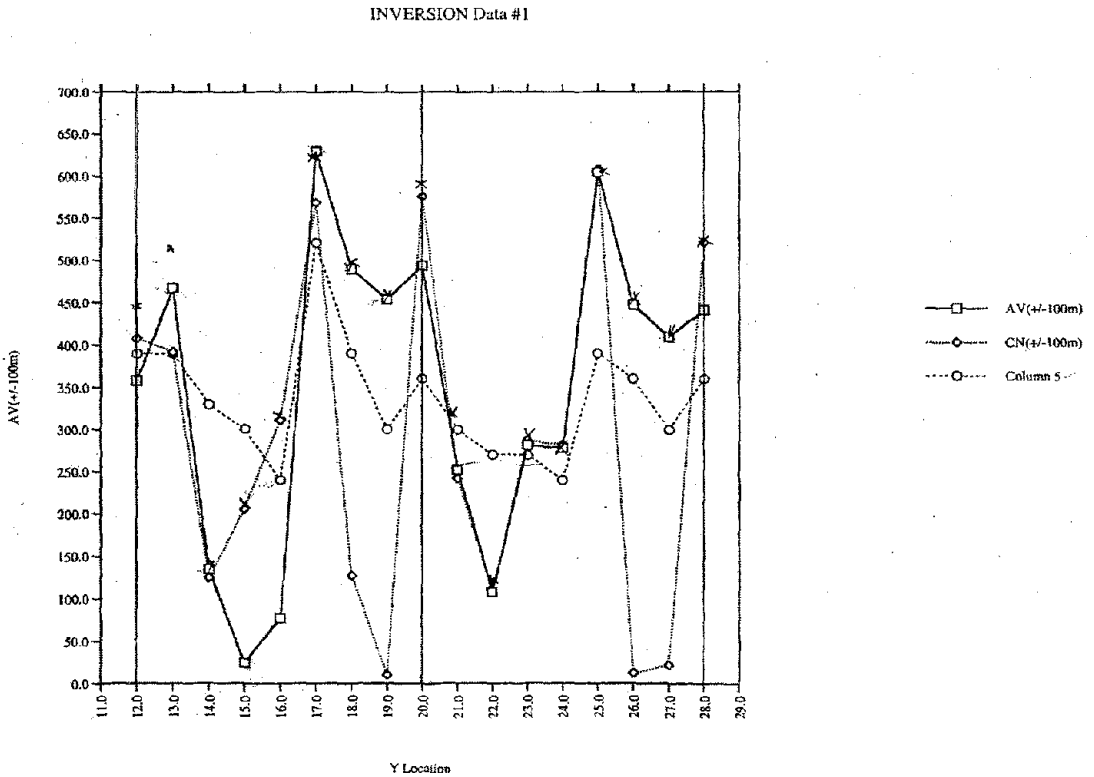
INVERSION Data #1
AV(+/-100m)
700.0
650.0
600.0
550.0
500.0
450.0
400.0
350.0
300.0
250.0
200.0
150.0
100.0
50.0
0.0
11.0
12.0
13.0
14.0
15.0
16.0
17.0
18.0
19.0
20.0
21.0
22.0
23.0
24.0
25.0
26.0
27.0
28.0
29.0
Y Location
AV(+/-100m)
CN(+/-100m)
Column 5

Figure 2a

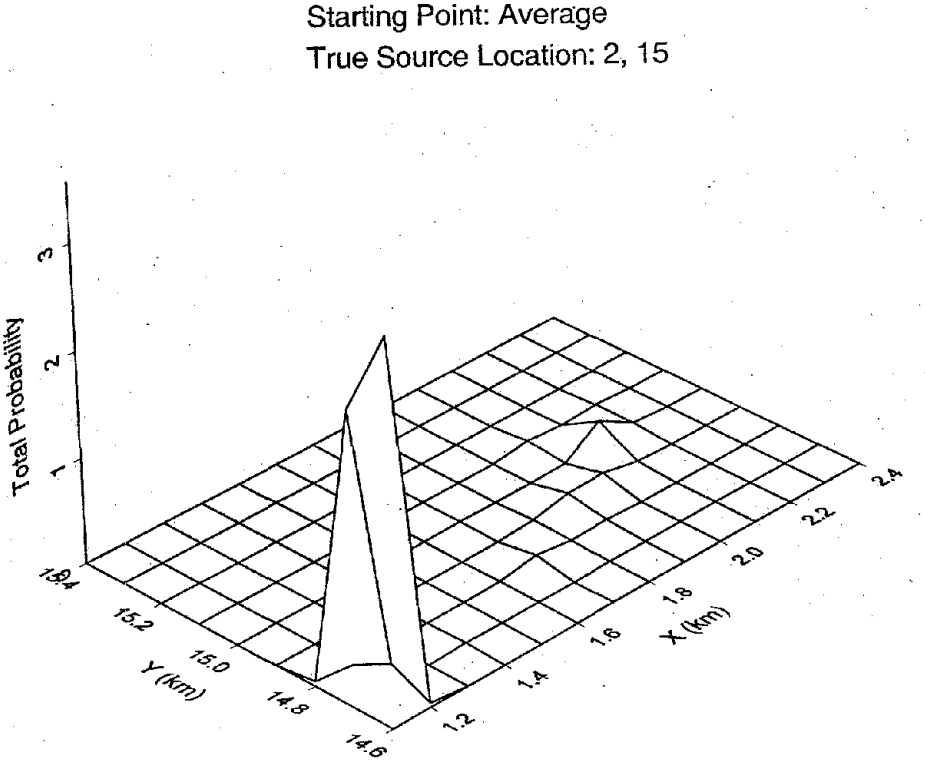

Figure 2b

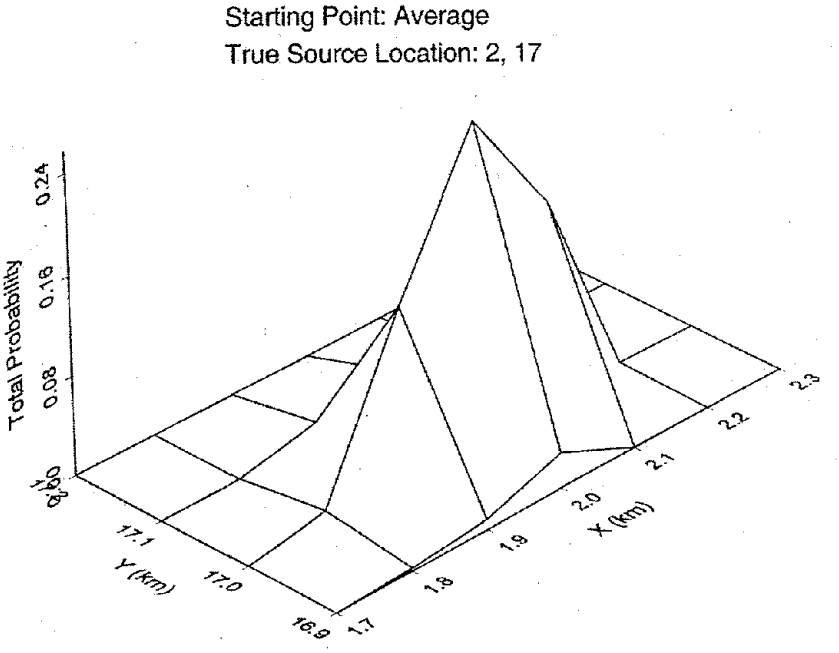

Figure 2c

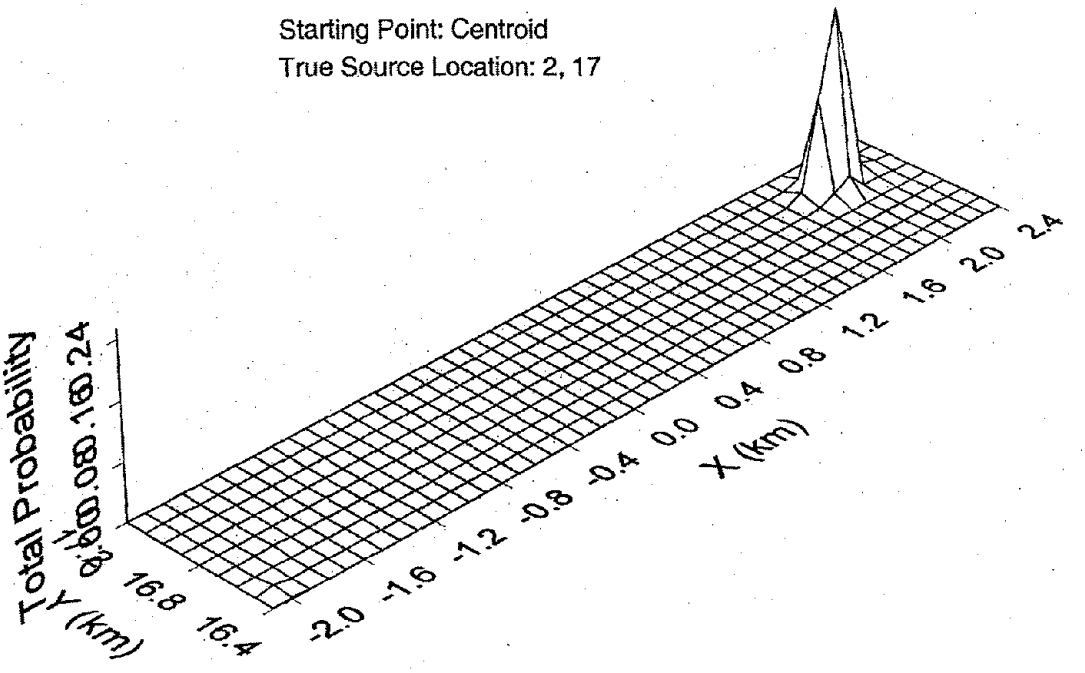

Figure 2d

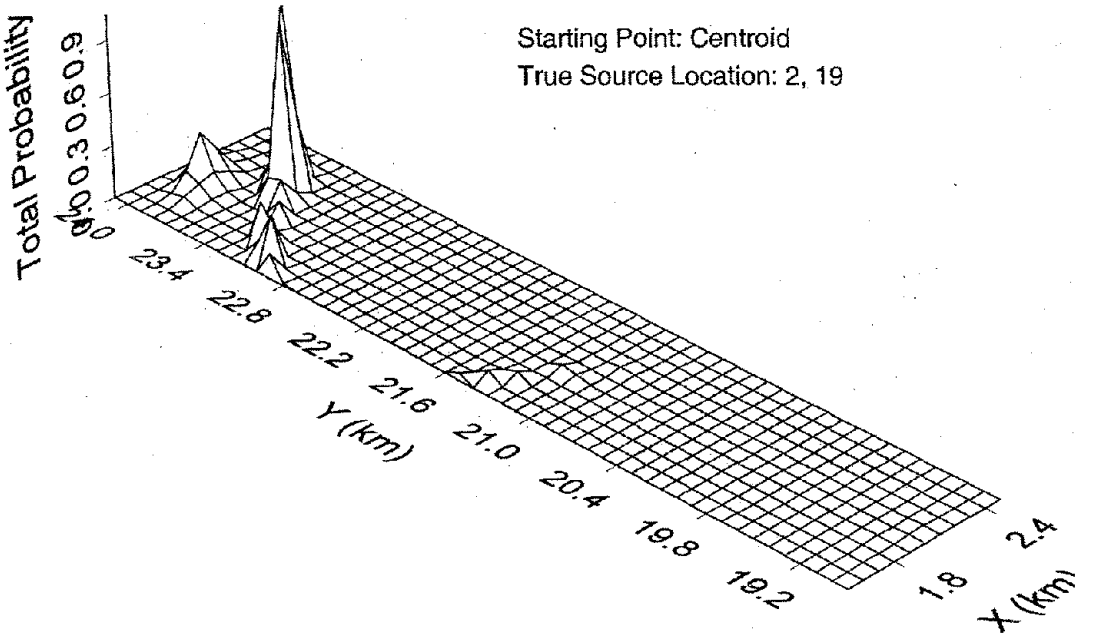

Figure 2e

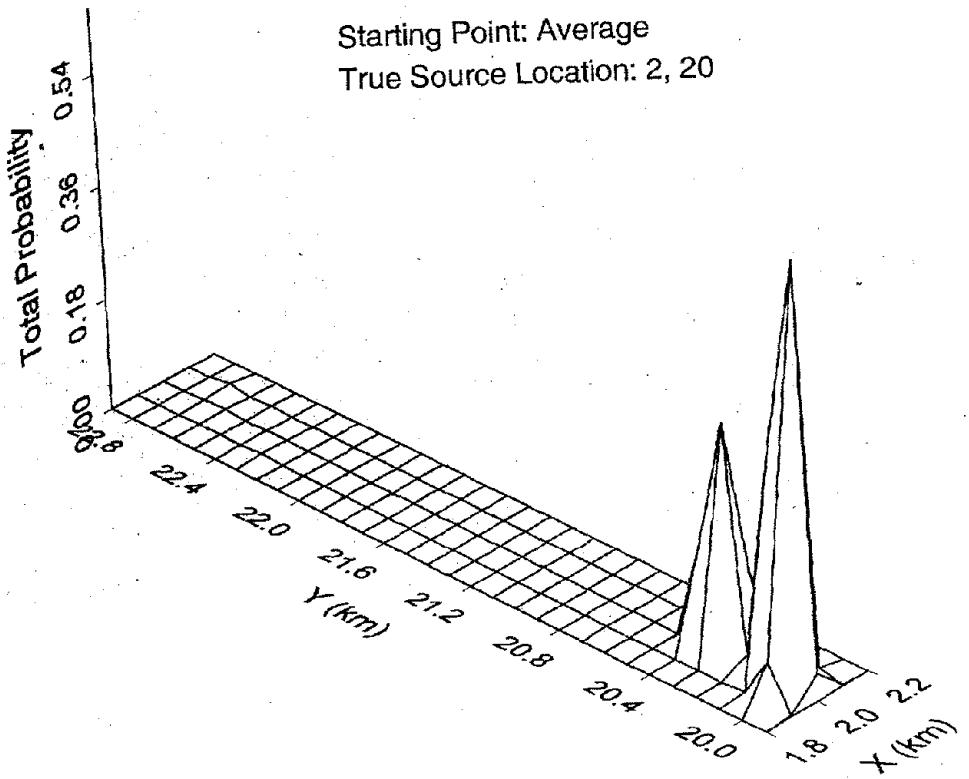

Figure 2f

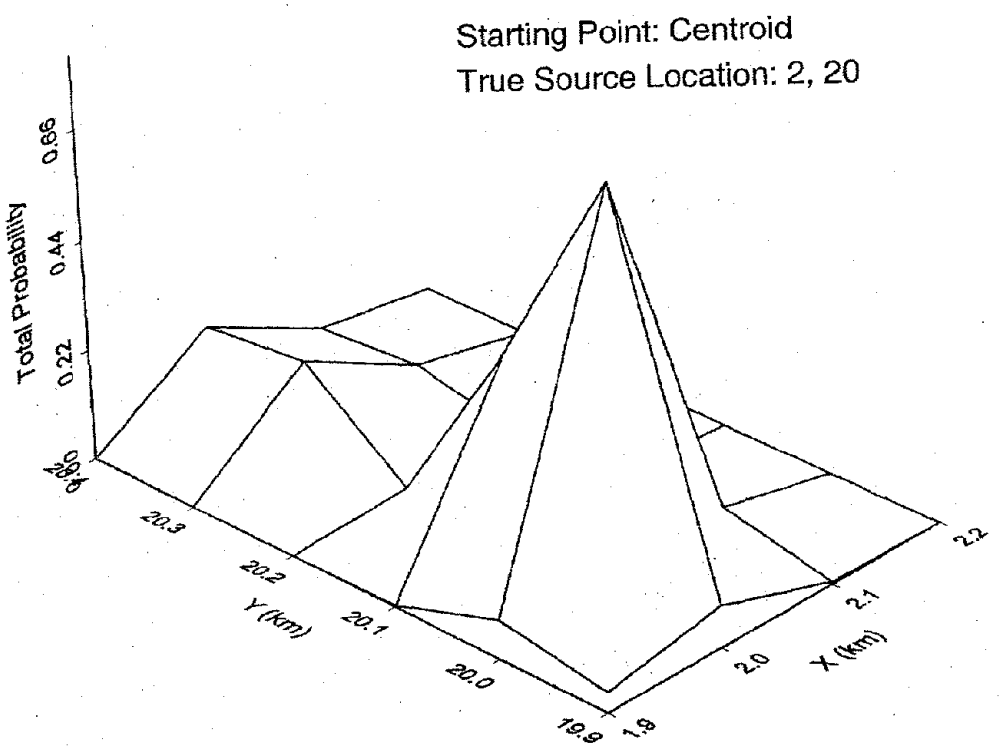

Figure 3a

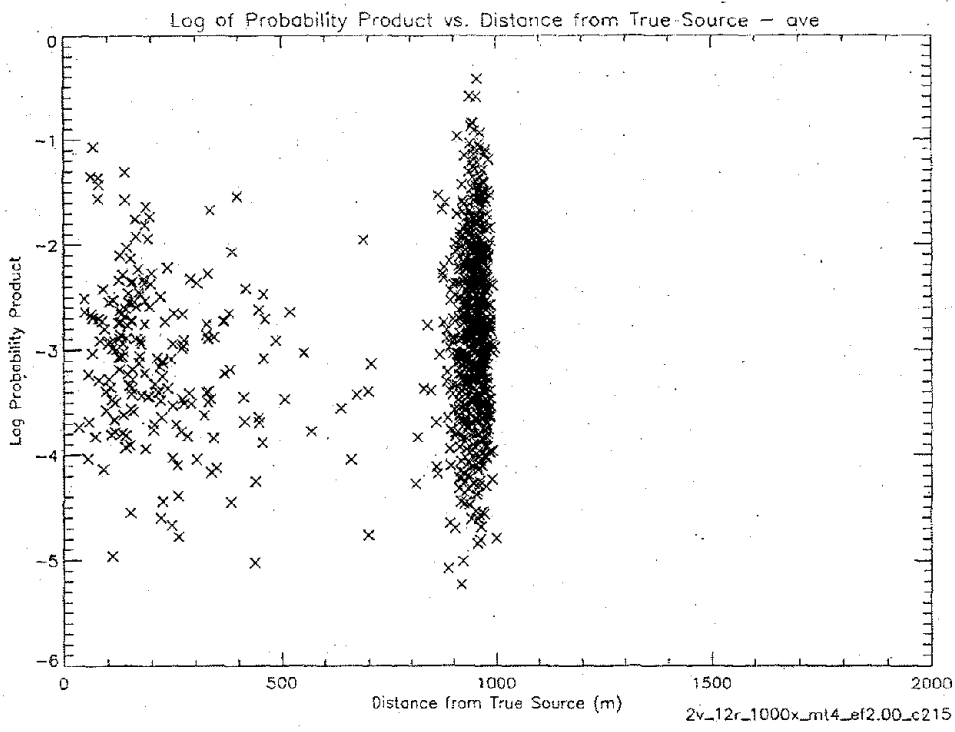

Figure 3b

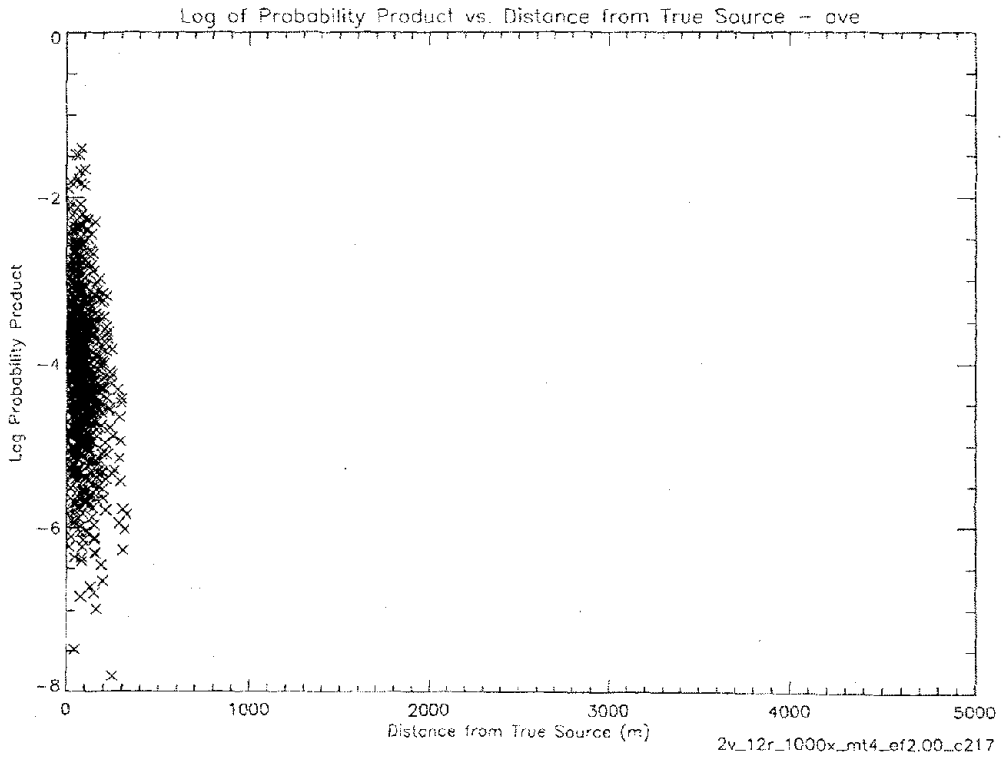

Figure 3c

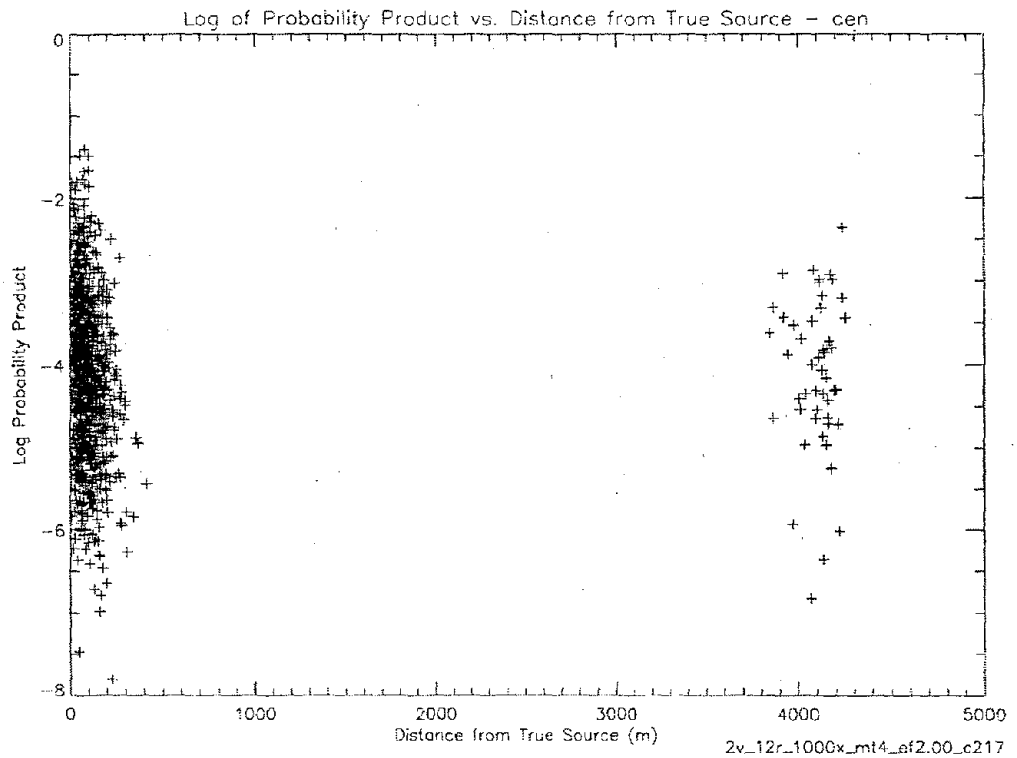

Figure 3d

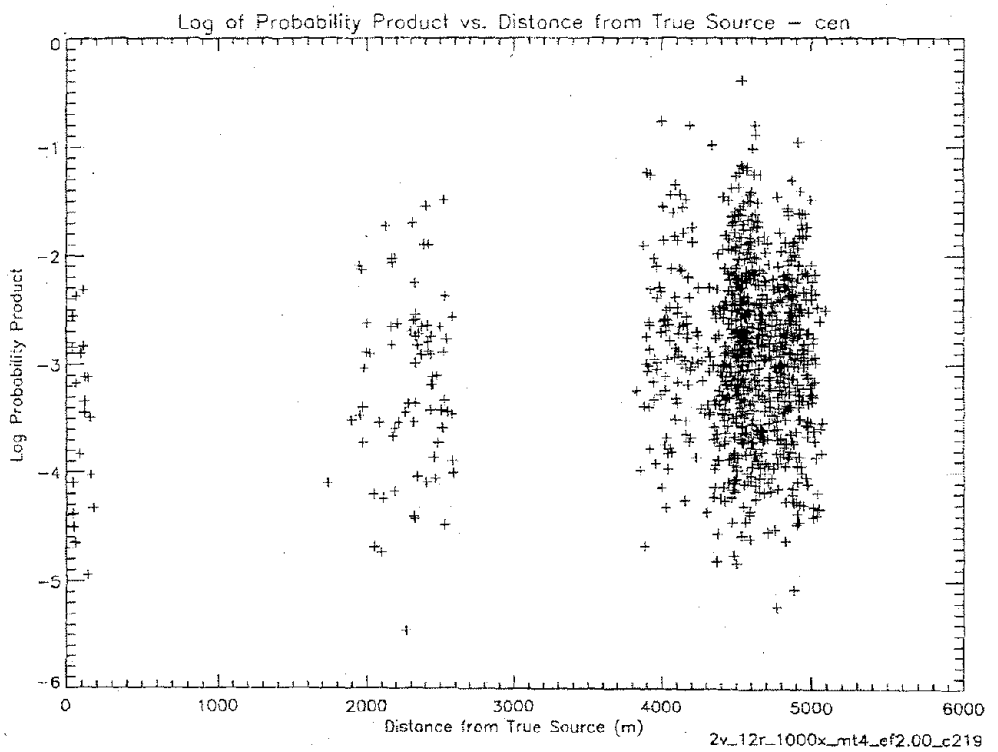

Figure 3e

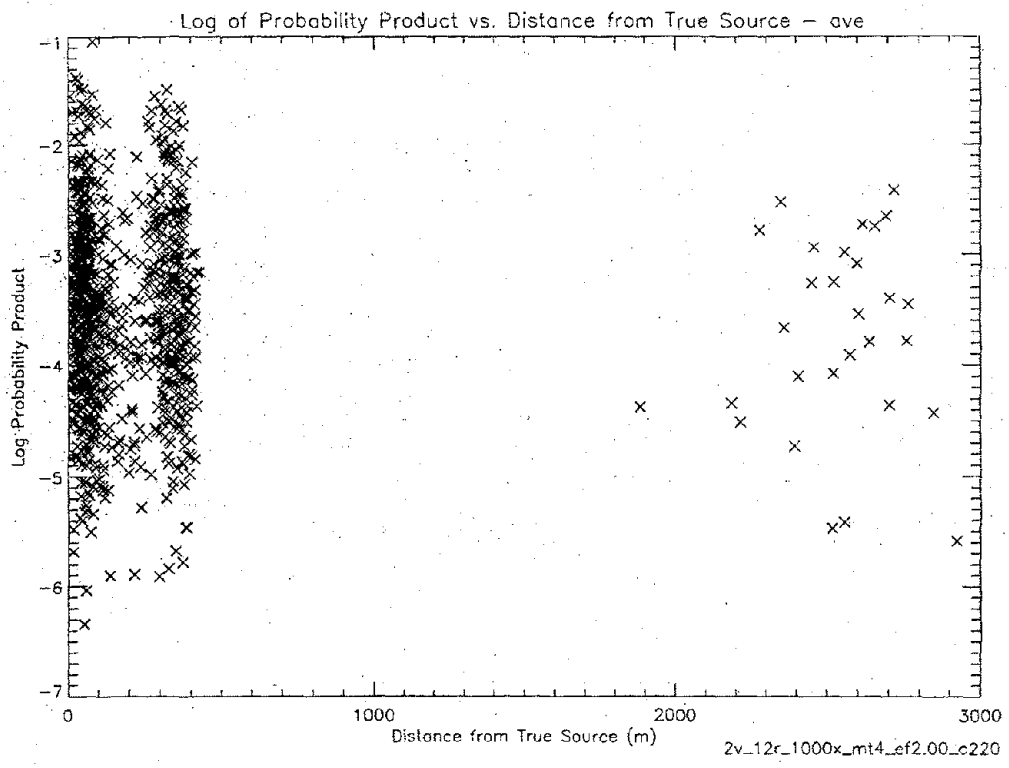

Figure 3f

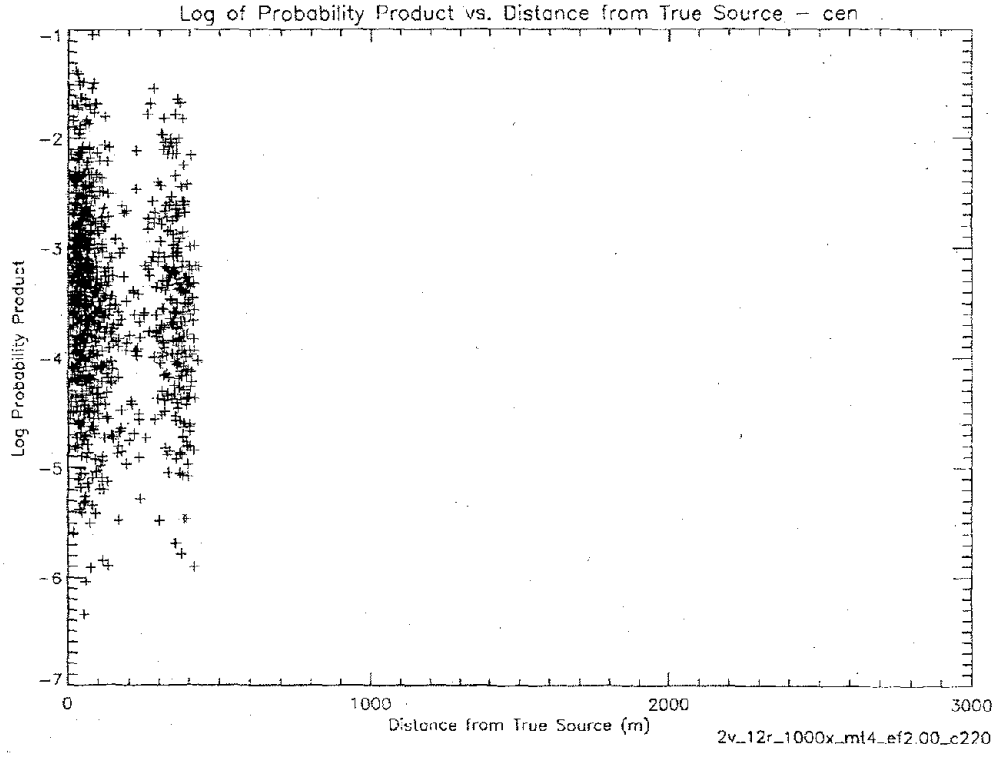

Figure 4a

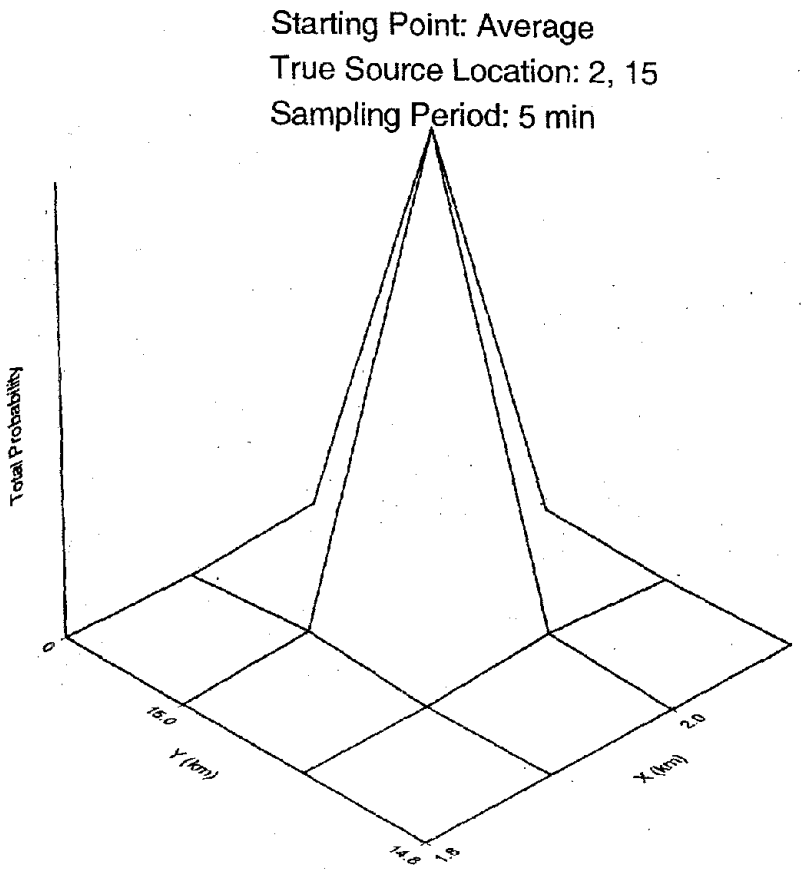

Figure 4b

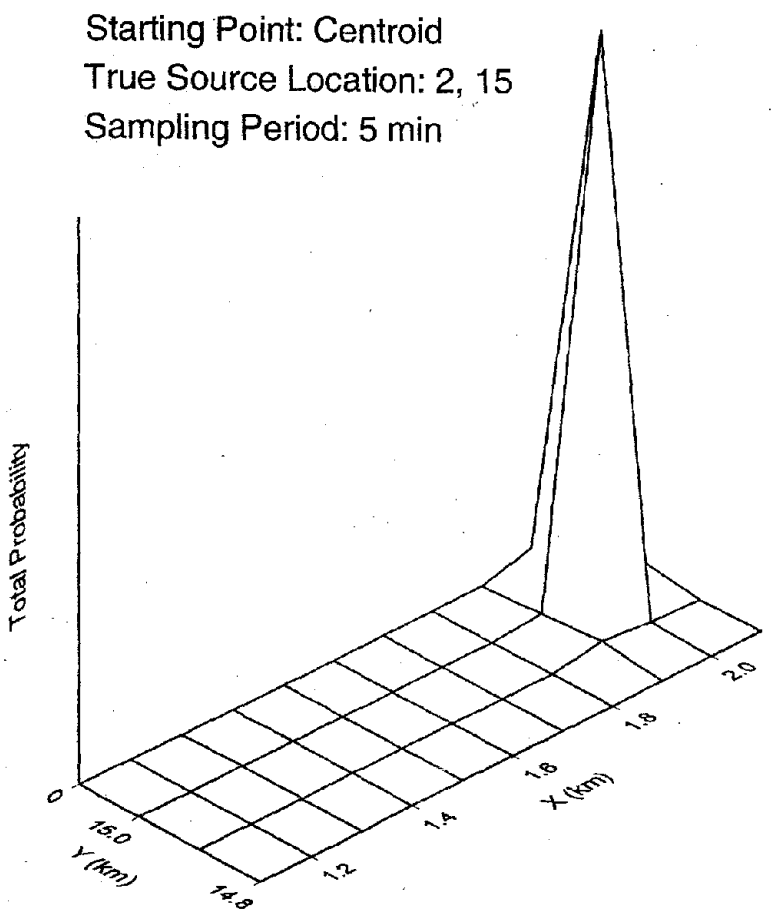

Figure 5a

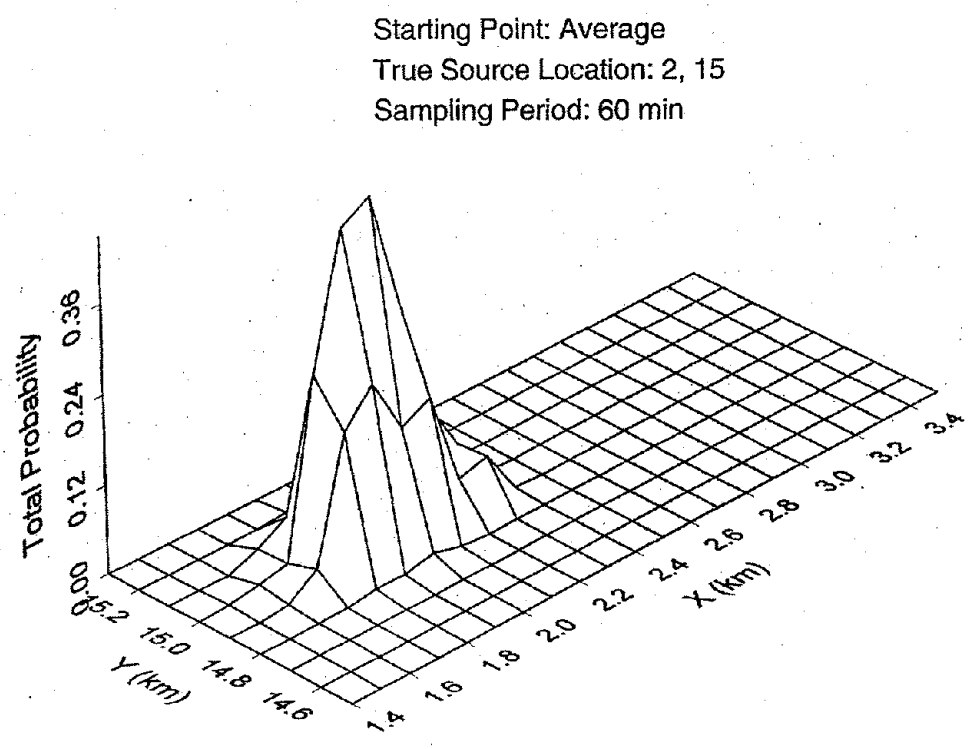

Figure 5b

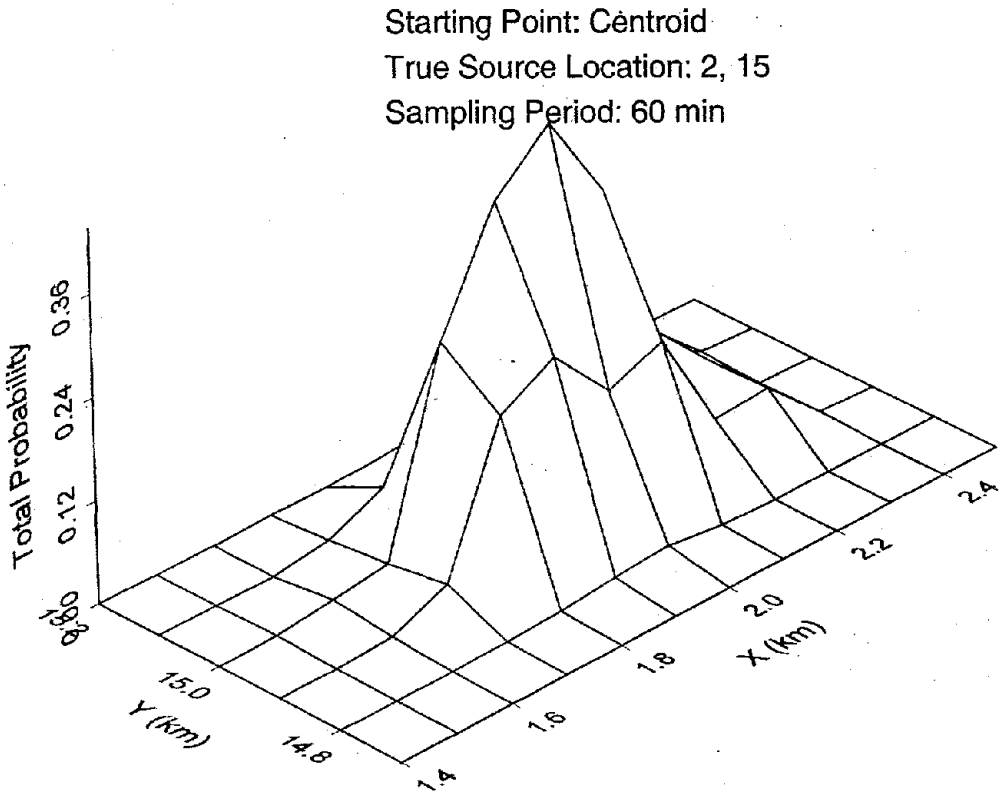

Figure 6a

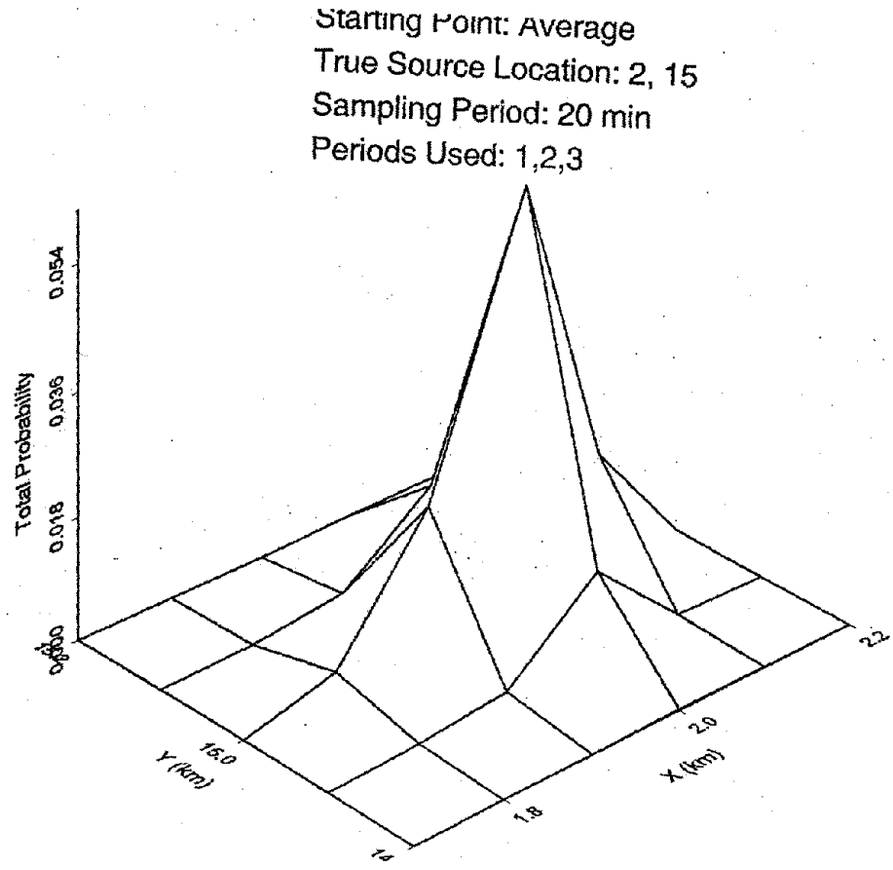

Figure 6b

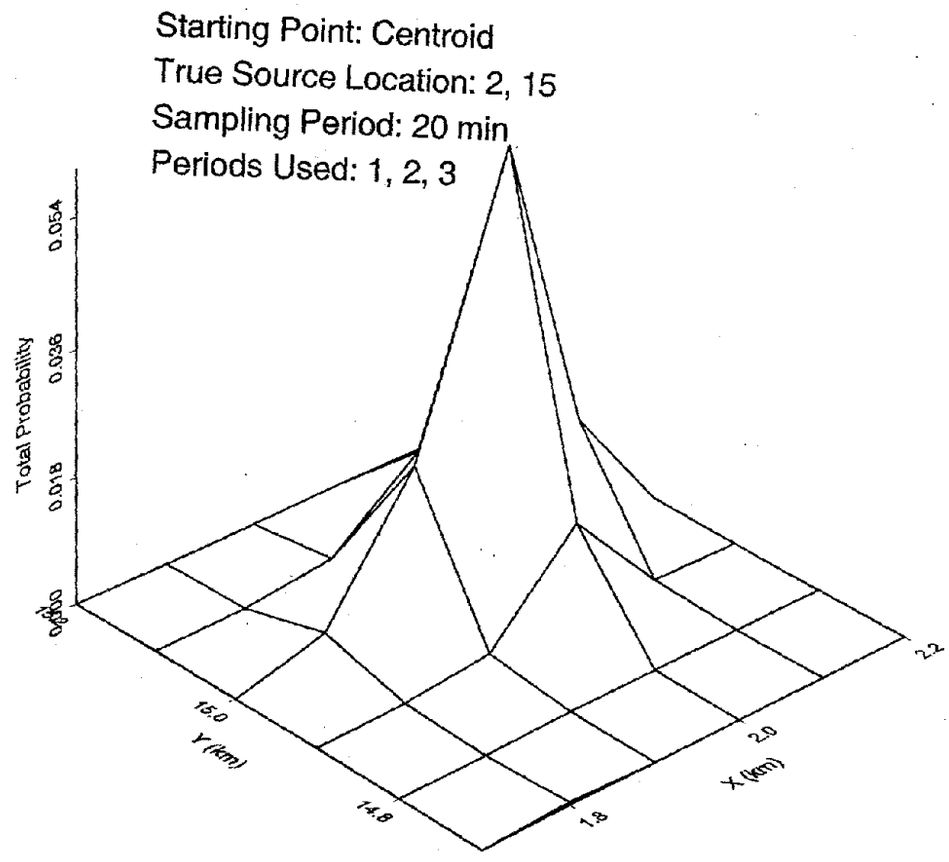

Figure 7a

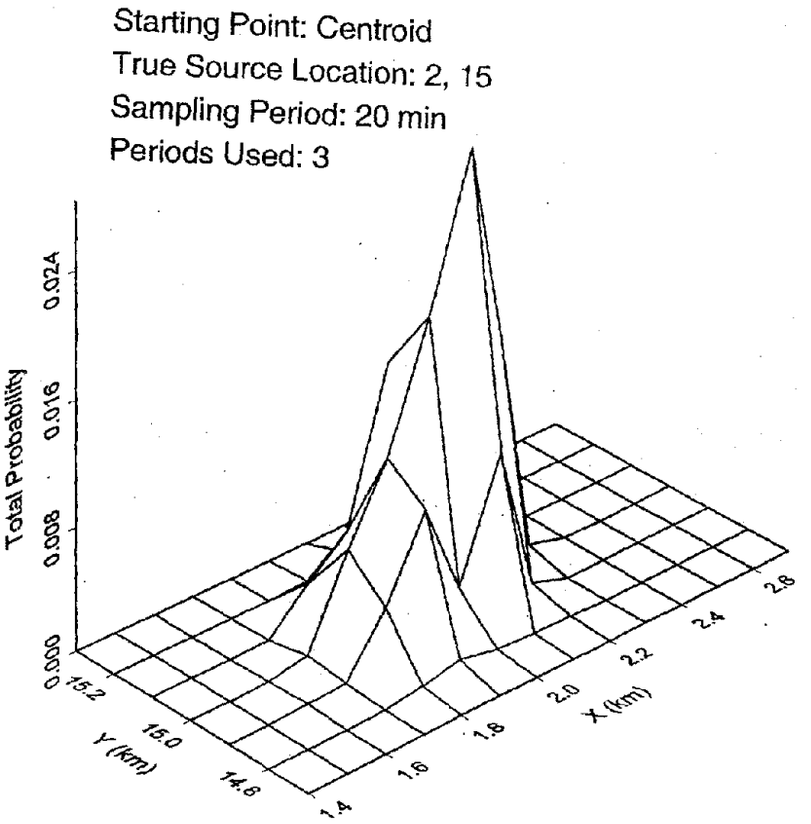

Figure 7b